Proceedings of the ASME 2013 7th International Conference on Energy Sustainability & 11th Fuel Cell Science, Engineering and Technology Conference
ESFuelCell2013
July 14-19, 2013, Minneapolis, MN, USA

ES-FuelCell2013-18245

COMPENSATION OF GRAVITY INDUCED HELIOSTAT DEFLECTIONS FOR IMPROVED OPTICAL PERFORMACE

James K. Yuan[1], Joshua M. Christian[2], and Clifford K. Ho[1]
[1]Concentrating Solar Technologies Department
Sandia National Laboratories
[2]Concentrating Solar Technologies Department
Sandia Staffing Alliance

P.O. Box 5800, MS-1127
Albuquerque, New Mexico, 87185 USA
Contact: ckho@sandia.gov

ABSTRACT

Heliostat optical performance can be affected by both wind- and gravity-induced deflections in the mirror support structure. These effects can result in decreased energy collection efficiency, depending on the magnitude of structural deflections, heliostat orientation and field position, and sun position. This paper presents a coupled modeling approach to evaluate the effects of gravity loading on heliostat optical performance, considering two heliostat designs: The National Solar Thermal Test Facility (NSTTF) heliostat and the Advanced Thermal Systems (ATS) heliostat. Deflections under gravitational loading were determined using finite element analysis (FEA) in ANSYS Mechanical, and the resulting deformed heliostat geometries were analyzed using Breault APEX optical engineering software to evaluate changes in beam size and shape. Optical results were compared against images of actual beams produced by each respective heliostat, measured using the Beam Characterization System (BCS) at Sandia National Laboratories. Simulated structural deflections in both heliostats were found to have visible impacts on beam shape, with small but quantifiable changes in beam power distribution. In this paper, the combined FEA and optical analysis method is described and validated, as well as a method for modeling heliostats subjected to gravitational deflection but canted in-field, for which mirror positions may not be known rigorously. Furthermore, a modified, generalized construction method is proposed and analyzed for the ATS heliostat, which was found to give consistent improvements in beam shape and up to a 4.1% increase in Annual Incident Power Weighted Intercept (AIPWI).

INTRODUCTION

A typical heliostat consists of a support structure made up of beams and trusses, on which a reflective surface is mounted. Construction of the structure and alignment of the reflective surface must be extremely precise to enable accurate reflection of incident power onto a receiver hundreds of meters away. However, because of the large number of heliostats needed in a concentrated solar power plant, heliostats must be designed to optimize structural stiffness with respect to material use, to maximize optical performance for minimal cost.

Figure 1: Representative heliostat designs. NSTTF heliostat (left) and ATS heliostat (right)

Figure 1 shows two representative heliostat designs: the 37 m^2 National Solar Thermal Test Facility (NSTTF) heliostat and the 149 m^2 Advanced Thermal Systems (ATS) heliostat. The NSTTF heliostat is a robust prototype structure configured for experimental purposes, whereas the ATS heliostat is representative of a typical production heliostat, including all commercial design considerations.

Finite element analysis (FEA) of heliostat structural deflection under arbitrary loading configurations can be

accomplished using commercial structural analysis codes, such as ANSYS Mechanical and SolidWorks Simulation. The approach of simulating entire heliostat structures using FEA was described previously by Moya and Ho [1], and accuracy was verified against measured deflections for experimental load cases. Structural deflections under gravitational loading alone may also be performed for arbitrary heliostat orientations.

Optical analysis software can be used to analyze the behavior of various reflective and absorbing objects when subjected to light sources, by tracing a finite number of light rays as they interact with optically defined surfaces in a modeled 3D environment. Furthermore, the power incident on or reflected from a surface can be quantified in simulation. By modeling the sun as a light source with a characteristic size and power emission, a simulation of an entire heliostat beam may be performed using the 3D geometry of a heliostat, field coordinates, and a target.

This paper describes a method for simulating the optical performance of heliostats after being subjected to gravitational loading in FEA, and introduces a recommendation for constructing heliostats to best counteract gravity deflection and improve beam quality.

NOMENCLATURE

A	Emitter area, m^2
DNI	Direct normal irradiance, W/m^2
P	Emitted power, W
cos	Cosine loss factor
$Cone\ angle$	Cone angle, radians
$HelioEl$	Heliostat elevation angle, degrees
$HelioAz$	Heliostat azimuth angle, degrees
φ	Angle between adjustment acceleration and heliostat mirror plane, degrees
θ_{ElW}	Power weighted elevation angle, degrees
$\theta_{El,Az}$	Power weighted orientation angles, degrees

MATERIALS AND METHODS

To investigate the effects of structural deflections on beam shapes, computer-aided design (CAD) models of the NSTTF and ATS heliostats were created. Geometries were produced in SolidWorks from the original engineering drawings for each heliostat, including all components and with all material properties rigorously specified. Models were then transferred to ANSYS Mechanical for meshing and FEA to obtain structural deflections for various heliostat orientations under gravity loading. The computational mesh consisted of approximately 1.5 million elements distributed across each heliostat model, with contact conditions between components chosen to best represent the physical case. Adhesive and weld joints were modeled as rigorously bonded, while bolted and simply supported components were given the appropriate degrees of freedom. Figure 2 shows ANSYS Mechanical models of the NSTTF and ATS heliostats.

In this study, three heliostat configurations were of interest for subsequent optical analyses:

1. The un-deformed heliostat. This case assumed no gravitational loading, and utilized the original geometries prior to FEA. This replicated the ideal case of a beam produced by a completely rigid heliostat of a particular design, at a given field position.
2. The gravity-deformed heliostat. This case utilized the heliostat shapes attained after simulated gravity loading, for a number of heliostat orientations corresponding to the orientations assumed throughout a day of tracking the sun. Optical analysis of these gravity deflected heliostat shapes was used to model the beams produced by a heliostat constructed to specifications but influenced by gravity sag.
3. The as-built, gravity-loaded case. This case modeled the shape of a heliostat when affected by gravity but canted in-field or during assembly to counteract imperfections in the support structure. This captures the additional deflections introduced when the heliostat rotates to a new orientation, such that both gravity and the adjustments made to counter gravity shift the mirrors away from their designed orientations rather than neutralize each other. Details of this modeling approach are described below.

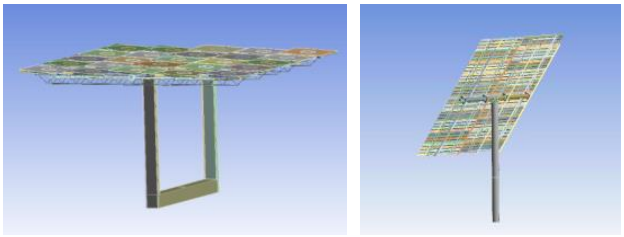

Figure 2: NSTTF (left) and ATS (right) heliostat models in ANSYS Mechanical

Heliostat canting may be performed in the field or during assembly such that mirrors are aligned to specifications regardless of gravitational deformations in the support structure, for one heliostat orientation. However, as the heliostat moves out of the orientation in which mirror alignment was performed, gravitational acceleration acts in a different direction relative to the structure, while the mirror adjustments made to nullify deflections remain fixed, causing the adjustments to no longer cancel the effects of gravity. This deformation is difficult to model because the final mirror adjustments may have been performed using mechanical or optical verification techniques, such that the specific dimensions needed to specify mirror positions in CAD are no longer known. By assuming small, linear deformations, this situation can be represented by applying an adjustment acceleration equal and opposite to gravitational acceleration during the FEA, to cause an initial deformation in the heliostat mirrors. When standard gravitational acceleration is applied, this initial deformation is neutralized and mirror positions return to their design point orientations. The adjustment acceleration remains at a fixed angle relative to the heliostat

mirrors (Figure 3), such that when the heliostat is rotated, the initial deformations caused by the adjustment acceleration are no longer equal and opposite to the deformations caused by gravity, and the heliostat assumes a separately deformed state. In this manner, it is possible to represent the shape of a heliostat that has been constructed to counteract gravity while in one specific orientation, and also the shapes attained after rotation to new orientations, without requiring specific dimensions to be known. Figure 3 shows a schematic of the modeling procedure.

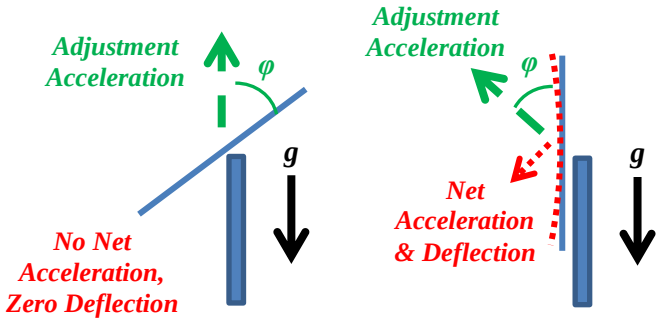

Figure 3: Schematic of modeling procedure for heliostat canted to counter gravitational deflection. Left: The canting orientation, with adjustment acceleration aligned with gravity, zero deflection. Right: rotated heliostat with adjustment acceleration not aligned with gravity with net acceleration and deflection

Optical performance of post-FEA heliostat shapes was evaluated in Breault APEX optical engineering software. This program is embedded within a CAD environment, allowing for the import of post-FEA deformed heliostat geometries for optical analysis. The optical model consisted of three components: a ray emission or sun source, the post-FEA heliostat geometry, and a power absorbing target, placed in the model environment to correspond to locations of the actual heliostats and tower at the NSTTF site (Figure 4).

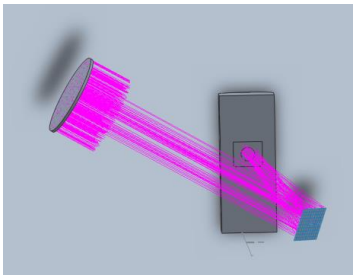

Figure 4: Optical model in Breault APEX, consisting of a sun source, the heliostat geometry, and a target

The ray emission source is a disk set to emit rays within a 9.3 mrad cone angle, to simulate the cone angle distribution of the sun observed from Earth. The total power being emitted from the source is defined in Equation 1.

$$P = DNI \times A \times \left(\frac{4}{(cone\ angle)^2}\right) \qquad (1)$$

Five million rays were traced from the source to ensure adequate resolution of simulated beams, and convergence of calculated reflected power was confirmed by running traces with lower and higher numbers of rays. The elevation and azimuthal angles of the modeled sun were calculated using Duffie [2] for each simulated time of day and date and each respective heliostat location on Earth. Similarly, the power emitted in Equation 1 was adjusted for expected DNI values based on location and time. For comparison against actual beams, mirrors can be implemented with slope error to model effects such as manufacturing defects and cleanliness. The power absorbing target used in this analysis was a simple flat surface with annular reference surfaces to evaluate the number of rays incident on specific areas. This allowed relative comparison of power and beam size from different deformed heliostat geometries.

RESULTS

NSTTF Heliostat

Figures 5-7 compare simulated beams from the NSTTF heliostat between -2 and +2 hours from solar noon for several times of year, from the un-deformed heliostat and from the gravity deformed shape. The simulated heliostat was located at the NSTTF site in Albuquerque, New Mexico, 131.7 m west and 136.9 m north of the tower, aimed at a point 28.9 m high on the tower. Individual facets were aligned to produce the best possible beam during solar noon on the equinox, and were focused to the target slant range. No slope error was included to best reveal gravity induced beam variations.

Gravitational deflection was found to have a minimal effect on beams produced by the NSTTF two hours before and during solar noon on the equinox. A decrease in peak flux and some shape change was seen in the gravity deformed beam image two hours after solar noon.

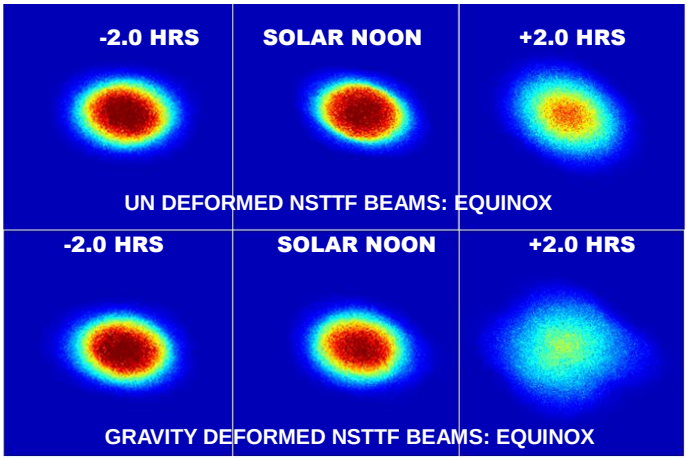

Figure 5: Simulated NSTTF beam images from un-deformed and gravity deformed heliostat models during equinox. Plot window dimensions are 7m x 7m

During summer solstice, a slight decrease in beam size was seen for the gravity deformed beam during solar noon (Figure 6). This demonstrates how gravitational deflections can sometimes cause an *increase* in performance by bringing mirrors closer to their optimal positions for a particular time of day. The gravity deformed beam two hours after solar noon showed increased spread, with a pattern similar to that seen during equinox.

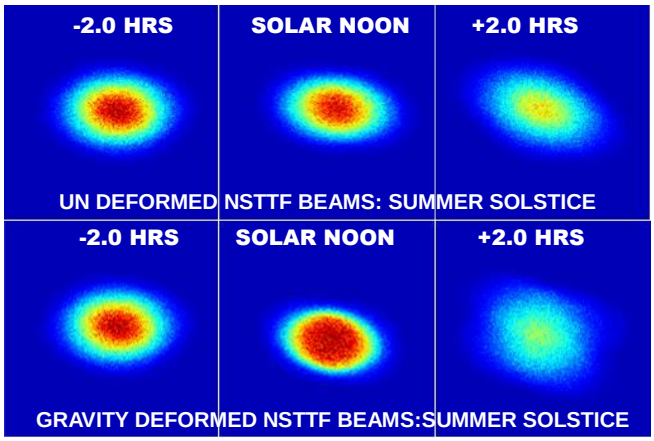

Figure 6: Simulated NSTTF beam images from gravity deformed and un-deformed heliostat models for various times of day during summer solstice. Plot window dimensions are 7m x 7m

During winter solstice, beams before and at solar noon showed minimal gravity induced-deformation. Small changes in shape were visible for beams produced 2 hours after noon (Figure 7).

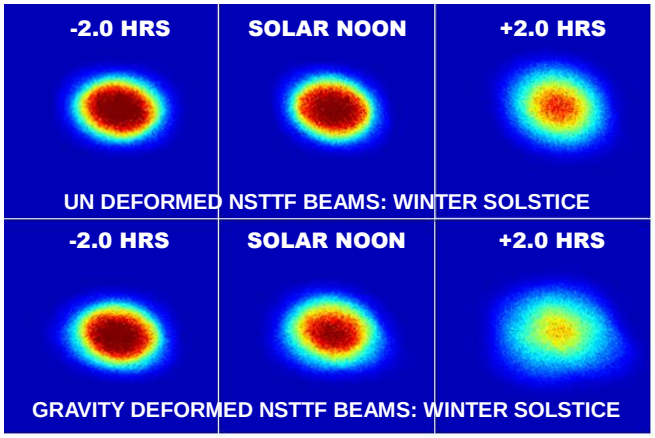

Figure 7: Simulated NSTTF beam images from gravity deformed and un-deformed heliostat models for various times of day during winter solstice. Plot window dimensions are 7m x 7m

Validation of the FEA and optical model was performed by comparing simulated beam images from the as-built, gravity-loaded NSTTF heliostat model against images obtained using the Beam Characterization System (BCS) at Sandia National Laboratories using the actual heliostat in the field. Simulations were run with 1 mrad random slope error applied to the mirrors to match the best estimate of actual mirror slope error as provided by on-site test engineers. As seen in Table 1, simulated and actual beams show a qualitative match, though the actual beam two hours after solar noon shows some elongation along its diagonal, a feature not seen in simulation. This can best be attributed to minor canting errors in the actual heliostat not captured in the model.

Table 1: BCS Beam Images vs. Simulated Beams from NSTTF Heliostat, Day 194, NSTTF Site, Albuquerque, NM

Hours from noon	BCS Image	Beams from simulated NSTTF heliostat
-2.0 HRS	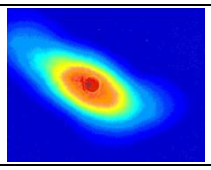	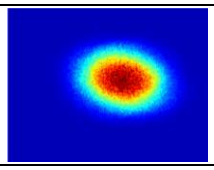
0.0 HRS	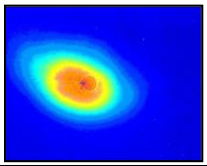	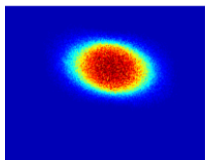
+2.0 HRS	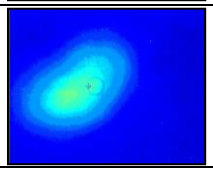	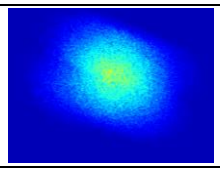

ATS Heliostat

Figures 8-10 compare beams from the un-deformed and gravity deformed ATS heliostat near solar noon for several times of year. The simulated heliostat was located at the NSTTF site, 19.0 m west and 235.0 m north of the tower, aimed at a point 28.9 m high. Facets were aligned and focused in rows of 5 to the slant range to the target. No slope error was included to best reveal beam variations caused by gravity.

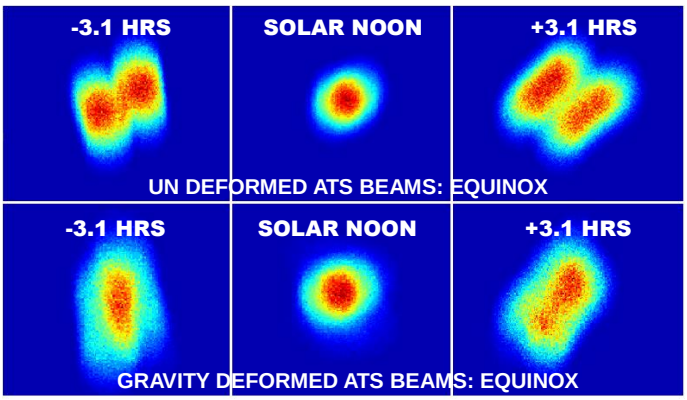

Figure 8: Simulated ATS beam images from gravity deformed and un-deformed heliostat models for various times of day during equinox. Plot window dimensions (hxw) are 9.0m x 10.5m

Gravitational deflection was found to have a visible impact on beam shape for the ATS heliostat. Beams were observed to diverge into two beams during off-noon hours, primarily due to the ATS being constructed of two halves, each with grouped facets such that only the center facet in each row of five facets was exactly aligned. This behavior is further emphasized by the exclusion of mirror slope error. Under gravity deformation, beams were seen to distort but beams from each heliostat half converged (Figure 9).

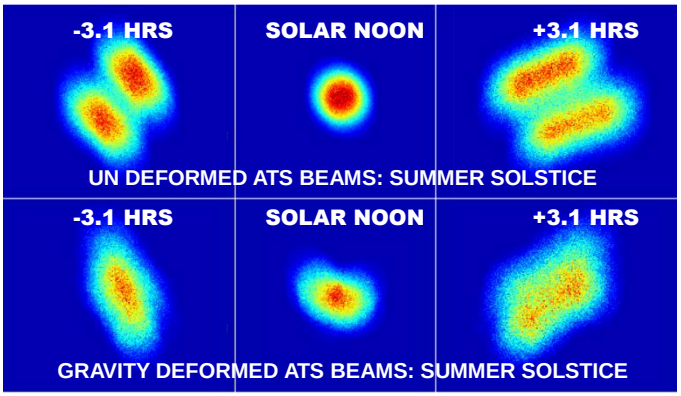

Figure 9: Simulated ATS beam images from gravity deformed and un-deformed heliostat models for various times of day during summer solstice. Plot window dimensions (hxw) are 9.0 m x 10.5 m

Divergence of beams from each half of the heliostat was also observed during winter solstice. Gravity deformation again caused some degree of convergence, as well as distortion of individual beam shapes (Figure 10).

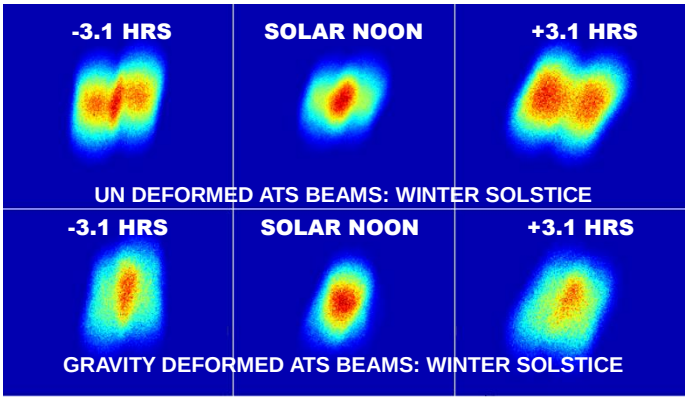

Figure 10: Simulated ATS beam images from gravity deformed and un-deformed heliostat models for various times of day during winter solstice. Plot window dimensions (hxw) are 9.0 m x 10.5 m

Validation of the ATS FEA and optical model was performed by comparing simulated beams from the as-built, gravity loaded ATS heliostat model with beams from the actual ATS heliostat at the NSTTF site. This configuration consisted of the heliostat model with an adjustment acceleration applied to neutralize deflection when the heliostat was oriented for noon equinox, to model the actual, on-sun canted heliostat. Because the ATS heliostat was not operational at the time of this study, simulated beams were compared against beam contour plots from previous tests [3]. Simulations were performed with 2 mrad random slope error applied to modeled mirror surfaces, matching estimates of slope error made by Strachan and Houser [3]. Table 2 shows simulated beams vs. contour plots of the measured BCS beam for the ATS heliostat.

Table 2: Simulated ATS Beams vs. Contour Plots of BCS Beams, Day 238, NSTTF Site, Albuquerque, NM

Time of Day	Contour plot from testing	Beams from simulated, as-built ATS heliostat
10:03 AM		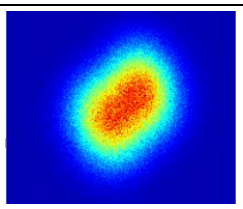
12:30 PM		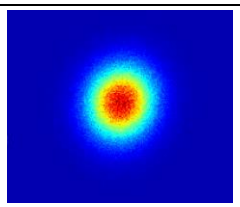
3:12 PM		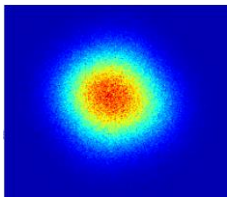
4:12 PM		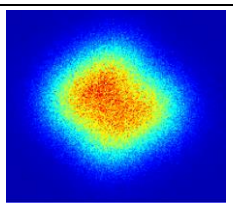
5:45 PM		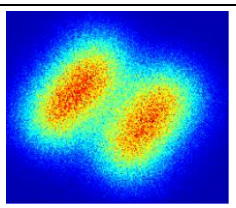

Simulated beam images showed a good qualitative match to contour plots of actual beams. Including the estimated random slope error on mirror surfaces tended to mask the beam divergence seen in the preceding analysis. Some beam divergence remained visible in the 5:45 pm simulation image. The slight rotation of the beam could be a result of deflection or imperfect alignment of the heliostat pedestal, a factor not considered in the model.

DISCUSSION

Beams from the NSTTF heliostat were found to be minimally affected by gravitational deflection. As seen in Figures 5-7, un-deformed and gravity deformed beams were visibly similar throughout the year, with total beam areas generally within 5% of each other. Thus, no gravity-induced beam spillage would be expected and the NSTTF heliostat structure can be considered sufficiently stiff with no need for structural improvements. However, the robust design of the structure is considered too expensive for commercial use.

The ATS heliostat was influenced by gravity sag more significantly than the NSTTF heliostat. However, the overall design represents a structure more suitable for use in commercial plants, at roughly 1/6 of the cost of the NSTTF structure per m^2 of reflective area [4]. The following discussion will be primarily applicable to heliostat designs for which ATS heliostat is representative, i.e. relatively lightweight heliostats with a T-shaped pedestal and torque tube configuration.

4.1 Gravity deformation as a function of elevation angle

As seen in Figure 8Figure 10, gravity induced beam deformation is an elevation angle dependent phenomenon. For the high elevation angles attained during summer solstice, mirrors are nearly horizontal and experience out-of-plane deformation, leading to different changes in beam shape than those observed during winter solstice when mirrors are nearly vertical and deform by shifting and rotating in-plane.

4.2 Power weighted average elevation angle

When canted in-field, heliostat mirrors are adjusted to their idea positions despite deformation in the substructure, for the heliostat orientation assumed during canting. For the ATS heliostat at the NSTTF site, canted off-axis to produce the best possible beam during solar noon on the equinox, this resulted in adjustments being made while the heliostat was at an elevation angle of approximately 30 degrees. However, when rotated to a nearly vertical (face forward) orientation, adjustments made to the heliostat while in the 30 degree canting orientation become too severe, as the component of heliostat deflection occurring out of the mirror plane is reduced. This results in a "clam-shelling" effect shown in Figure 11. Likewise, when rotated to an elevation angle greater than the canting orientation, gravitational acceleration acts out of the mirror plane to a magnitude greater than what was adjusted for, leading to sagging of the structure. Figure 11 illustrates modeled heliostat deformation modes for low and high elevation angles.

To best counteract this problem, it is proposed that heliostats be canted while oriented in the average elevation angle that is attained when maximum energy collection occurs, or a power weighted elevation angle, such that during times of peak energy availability the heliostat is at an elevation angle close to the angle in which it was canted. In this manner, the difference between canting adjustments and deflection directions is minimized, helping to maintain a nearly un-deformed heliostat with a minimally affected beam for the most energy-rich times of day.

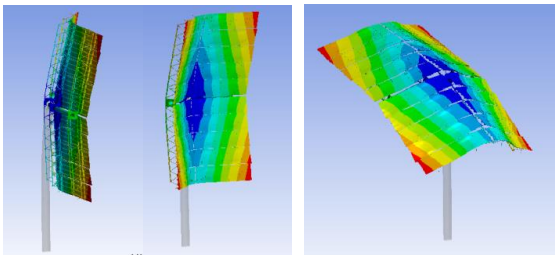

Figure 11: Heliostat deformed configurations when adjusted for no deflection at a single elevation angle. Left: "Clam-shelling" at elevation angles below the adjustment angle. Right: Sagging of structure at elevation angles above the adjustment angle. Peak deflection approximately 5 mm (scaled ~500X)

The power weighted elevation angle is developed in Equation 2 by averaging hourly heliostat elevation angles attained throughout a year, weighted by cosine loss and direct normal insolation (DNI) for a typical meteorological year [5]:

$$\theta_{ElW} = \frac{\sum_{i=1}^{8760} DNI_i * cos_i * HelioEl_i}{\sum_{i=1}^{8760} DNI_i * cos_i} \quad (2)$$

This power weighted average elevation angle can be found for every heliostat in a field, and is unique for each individual field position. Canting a heliostat while it is oriented in this elevation angle theoretically ensures that deflections will be minimized during times of year when energy collection potential is greatest. The use of a typical meteorological year allows seasonal variations in available power to be accounted for, in addition to the field and sun geometry parameters of (2). The power weighted elevation angle for the ATS heliostat was found to be 22.9°, lower than the noon equinox angle of 29.3°. It is important to note that this methodology simply implements a given canting strategy (i.e. on-axis, off-axis to solar noon on the equinox, etc.) with the heliostat in a carefully chosen elevation angle to minimize gravitational effects over the range of annual operational angles, but does not change the canting strategy used.

To evaluate the potential gains of implementing noon-equinox canting while oriented in the power weighted elevation angle versus in the noon-equinox orientation, ray traces were performed throughout a day for characteristic times of year for the heliostat under each implementation orientation. The power incident on a circular area two times the diameter of the smallest possible beam (the observed subtended angle of the sun multiplied by the target slant range) was used to find an intercept factor for the reflected heliostat power. This diameter was chosen as a representative receiver size scalable by field position. No mirror slope error was included in these simulations to better clarify any potential changes in beam power distribution. Figures 12-14 show the intercept factors for several times of day during equinox, summer solstice, and winter solstice, for the ATS heliostat at the NSTTF using each canting orientation.

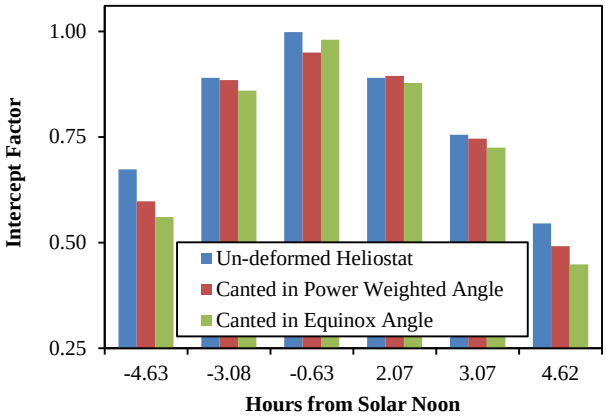

Figure 12: Intercept factors on a target two times the minimum theoretical beam size (~4.4 m), for various modeled ATS heliostat configurations during equinox

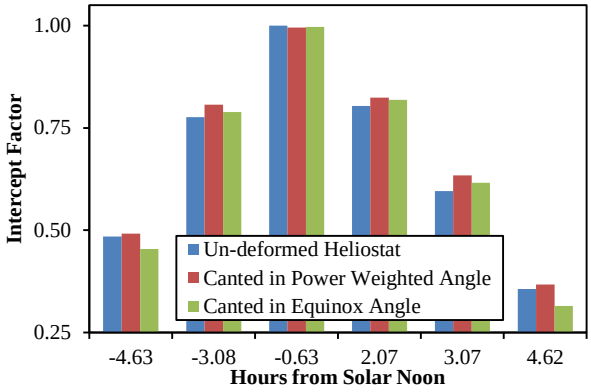

Figure 13: Intercept factors on a target two times the minimum theoretical beam size (~4.4 m), for various modeled ATS heliostat configurations during summer solstice

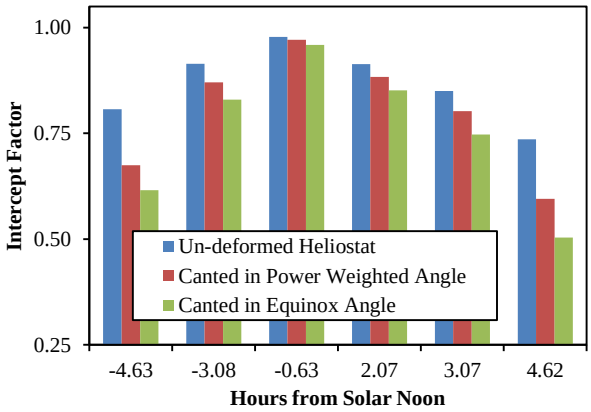

Figure 14: Intercept factors on a target two times the minimum theoretical beam size (~4.4 m), for various ATS heliostat configurations during winter solstice

The data from Figures 12-14 was used to evaluate a daily power weighted intercept factor. Power at each simulated time of day away from solar noon varied according to a 30-day average hourly power distribution from TMY data, centered on the simulated day of the year for which the daily intercept factor was being calculated. A piecewise linear fit between daily power weighted intercept factors was then produced to interpolate intercept factors for each day of the year, shown in Figure 15. An estimate of annual incident power weighted intercept (AIPWI) was then found, again on a target two times the minimum possible beam size, using the interpolated daily power weighted intercept factors and TMY data for daily insolation (Figure 15). This is slightly distinct from a simple integration under the daily power weighted intercept factors, since seasonal variations in insolation over the year are accounted for.

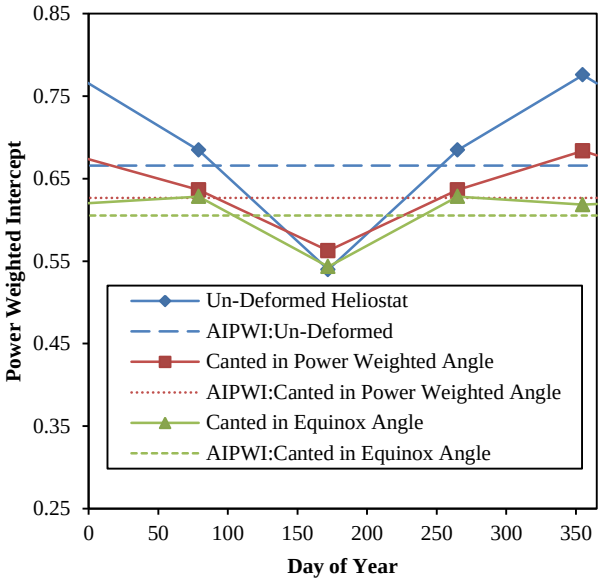

Figure 15: Daily and annual power weighted intercept factors on a target two times the minimum beam size (~4.4 m) for various modeled ATS heliostat configurations

As shown in Figure 15, heliostat cases including gravity loading showed loss of efficiency compared to the ideal, un-deformed case. During summer, high cosine losses near noon reduced midday power collection despite excellent intercept, leading to a reduction in the noon intercept weighting factor. This subsequently allowed more weight to be placed on off-noon times of day with low intercept (Figure 13), leading to the poor overall power weighted summertime intercept factor seen in Figure 15. Deformations were reduced during winter solstice when heliostat elevation angles were lower and closer to the power weighted elevation angle, leading to an increase in off-noon intercept factors, as seen in Figure 13. In addition to lower cosine losses, this contributed to the high power weighted intercept factors observed in Figure 15 during winter. The overall AIPWI for a heliostat canted while oriented in the power weighted elevation was 0.627, higher than 0.603 as when canted in the noon equinox orientation, producing a gain of 4.1%. The ideal un-deformed heliostat AIPWI was 0.666.

4.3 Notes on implementation

As opposed to canting a heliostat to produce an ideal beam during noon equinox while oriented in the noon equinox elevation angle (canting on-sun), the power weighted elevation angle method does not represent a physical situation as it assumes a heliostat is canted while oriented at a different elevation angle than the elevation angle attained at the instant in time when the implemented canting strategy produces the best possible beam. However, this is the case for any heliostat not canted on-sun. Additional FEA using one or more adjustment accelerations as shown in Figure 3 would enable the required mirror alignments to be found when it is desired for the heliostat to have no deformation while oriented in the power weighted elevation angle, but is placed in an orientation optimized for physical assembly. Alignment of mirrors could then be performed using existing optical and metrological methods with no change in the assembly process.

4.4 Discussion of further improvements

The preceding analysis showed that by performing canting while the heliostat is oriented in a strategically chosen angle, or by performing an equivalent adjustment during assembly, the annual power weighted intercept factor may be increased by whole percentage points since gravity induced deflections are reduced. The following includes strategies for further improvements and directions for future work.

Changing canting strategy

As seen in Figures 8-10, even the beams produced by an ideally rigid, un-deformed heliostat may show significant spread during off-noon hours for some times of day, as an unavoidable side effect of a canting strategy which can only align mirrors ideally for one instant in time, in this case solar noon during the equinox. Nonetheless, considering cosine losses at varying field positions and seasonal variations in insolation, a potentially more efficient instant in time for which to align mirrors could be developed similarly to Equation 2 by weighting the annual elevation and azimuthal angles attained by a heliostat with available power:

$$\theta_{El,Az} = \frac{\sum_{i=1}^{8760} DNI_i * cos_i * HelioEl_i, HelioAz_i}{\sum_{i=1}^{8760} DNI_i * cos_i} \qquad (3)$$

In this manner, the heliostat would be canted to produce the ideal beam while oriented in the power weighted average elevation and azimuthal angles it attains throughout a year, and would simultaneously minimize gravitational deflections for that average orientation. Although the azimuthal angle has no effect on gravity deflections, weighting by azimuth angle may help to bias the canting orientation toward times of day with lower cosine loss, particularly for significantly off-axis field positions. The average orientation described by (3) intersects at least one real orientation attained in time, giving a sun position to which facets may be aligned. Similar analyses describing the optimal instant in time for which to cant was presented by Buck and Teufel without regard to gravity deflections, along with other time-independent canting strategies such as on-axis and parabolic alignment [6], all of which may yield further improvements to beam quality if implemented with the heliostat oriented in its power weighted elevation angle.

Allowing for strategic gravity deformations

The analysis presented focuses on countering gravity induced deflections in heliostats as a way to improve performance. However, as seen in Figures 8-10, gravity deformations left unaccounted for may sometimes reduce beam area and increase performance, for certain heliostat orientations and times of year. The coupled FEA and optical analysis method presented herein may enable the design and evaluation of low-stiffness heliostats specifically designed to deform in such a way as to increase performance. This could allow for a simultaneous reduction in material cost and increase in performance, although wind deflection and structure survivability limits must still be considered.

CONCLUSIONS

This paper describes a method for simulating beams produced by heliostats affected by gravitational acceleration, using the NSTTF and ATS heliostats as representative designs. A method for modeling adjustments made during canting to counteract gravity effects was presented, along with a generalizable method for improving beam quality by reducing heliostat gravitational deflection.

The following conclusions may be drawn:

(1) Heliostat and beam deformation is elevation angle dependent. The direction that gravity acts in relative to the structure varies with elevation angle, and thus the degree of deformation in the structure and the resulting beam is variable.

(2) Every heliostat has a power weighted elevation angle, or an average angle in which it is oriented while collecting the most power over a year. Constructing a heliostat and aligning mirrors to counteract gravity while in this orientation angle results in the heliostat remaining less deformed during times of year when power availability is maximal. This does not affect the canting method (i.e. on-axis, off-axis, parabolic, etc.), serving only to reduce elevation angle dependent gravity deformation. Implementation of this method in simulation resulted in a 4.1% increase in AIPWI for a receiver 2 times the ideal beam produced by the ATS heliostat at the NSTTF site. Other canting strategies may allow for even greater improvements.

(3) Gravitational deflections were sometimes observed to cause a decrease in total beam area. Using the modeling methods presented in this paper it may be possible to exploit gravitational deformations such that beam quality can be improved for structures of deliberately reduced stiffness and lower cost.

However, wind deflection and structural survival must still be considered.

ACKNOWLEDGMENTS

Sandia National Laboratories is a multi-program laboratory managed and operated by Sandia Corporation, a wholly owned subsidiary of Lockheed Martin Corporation, for the U.S. Department of Energy's National Nuclear Security Administration under contract DE-AC04-94AL85000.

REFERENCES

[1] Moya, Adam C. and Ho, Clifford K. "Modeling and Validation of Heliostat Deformation Due to Static Loading". Proceedings of the ASME 2011 5th International Conference on Energy Sustainability & 9th Fuel Cell Science. ESFuelCell2011-54216. 2011.

[2] Duffie, J.A. and W.A. Beckman, 2006, Solar Engineering of Thermal Processes, 3rd Edition. Wiley. Hoboken, NJ, xix.

[3] Strachan, John W. and Houser, Richard M. "Testing and Evaluation of Large Area Heliostats for Solar Thermal Applications". Sandia National Laboratories. SAND92-1381UC. 1993.

[4] Winter, C.-J., Sizmann, R. L., Vant-Hull, L. L. "Solar Power Plants: Fundamentals – Technology – Systems - Economics", Springer-Verlag Berlin, Heidelberg. 1991.

[5] Typical Meteorological Year 3. National Solar Radiation Database. National Renewable Energy Laboratory. 2005. http://rredc.nrel.gov/solar/old_data/nsrdb/1991-2005/tmy3/

[6] Buck, R and Teufel, E. "Comparison and Optimization of Heliostat Canting Methods". Proceedings of the Energy Sustainability Conference. ES2007-36168. 2007.